*minerals*

MDPI

*Article*

# Parametric Study on APTES Silanization of Coal Fly Ash for Enhanced Rubber Composite Performance

**Dennis S. Moyo [1], George Kleinhans [1], Xueting Wei [1], Frédéric J. Doucet [1,2,*] and Elizabet M. van der Merwe [1,*]**

[1] Department of Chemistry, University of Pretoria, Lynnwood Road, Pretoria 0002, South Africa; dennis.moyo@up.ac.za (D.S.M.)
[2] Council for Geoscience, 280 Pretoria Street, Silverton, Pretoria 0001, South Africa
* Correspondence: fdoucet@geoscience.org.za (F.J.D.); liezel.vandermerwe@up.ac.za (E.M.v.d.M.)

**Abstract**

The surface modification of coal fly ash (CFA) with silane coupling agents improves its compatibility with polymer matrices and supports its use as a sustainable filler in composite materials. This study examined the effects of the solvent system, reaction temperature, and pH on the grafting of 3-aminopropyltriethoxysilane (APTES) onto CFA surfaces. Functionalization was assessed by Fourier-transform infrared spectroscopy (FTIR), focusing on the $CH_2$ symmetric and asymmetric stretching bands of pure APTES at 2919 and 2957 $cm^{-1}$, noting that a slight shift in these bands can be expected following the change in the local chemical environment upon grafting. Solvent mixtures containing water (ethanol/water, acetone/water, and sulfuric acid/water) produced stronger coupling than the toluene solvent, which indicated the importance of water for APTES hydrolysis and silanol formation. Coupling efficiency increased with temperature and reached a maximum at 80 °C, where the balance between hydrolysis and condensation favored the formation of stable Si–O–Si bonds. The highest degree of functionalization was observed at pH 9, which corresponds to the point of zero charge of alumina in CFA, where neutral surface hydroxyl groups were available to react with silanols. These results define the optimal conditions for APTES grafting onto CFA and demonstrate its potential as a silane-modified filler in polymer composites. Atomic force microscopy (AFM) provided direct visual evidence of significant surface texture modifications induced by APTES treatment in the ethanol/water solvent system.

**Keywords:** coal fly ash; silane coupling agent; 3-aminopropyl triethoxysilane; APTES; FTIR; grafting



Received: 30 September 2025
Revised: 9 November 2025
Accepted: 10 November 2025
Published: 14 November 2025

**Citation:** Moyo, D.S.; Kleinhans, G.; Wei, X.; Doucet, F.J.; van der Merwe, E.M. Parametric Study on APTES Silanization of Coal Fly Ash for Enhanced Rubber Composite Performance. *Minerals* **2025**, *15*, 1198. https://doi.org/10.3390/min15111198



## 1. Introduction

Silane ($SiH_4$) is the simplest molecular silicon hydride, consisting of one silicon atom covalently bonded to four hydrogen atoms. It serves as the basic building block for a wide range of silane derivatives, often called "silanes". Silanes are widely used in the chemical industry as coupling agents between two dissimilar materials, as surface modifiers for adhesion of various coatings, and as precursors in the production of high-purity silicon [1,2].

When silanes are used as coupling agents, they form a molecular bridge that enhances the adhesion between organic polymeric matrices and inorganic solids, such as mineral fillers, glass, metals and metallic oxides [3]. The surface treatment of fillers using silanes has a strong influence on the (1) physical interactions between the polymer and filler, which

control processing properties such as viscosity, filler dispersion and wetting efficiency [4]; (2) chemical interactions between the polymer and filler, which lead to improved aging and ultimate mechanical properties due to the formation of a strongly chemisorbed layer that protects the polymer/filler interface from hydrolysis; and (3) physical interaction between filler particles, which controls dynamic mechanical and rheological properties [5].

Silane coupling agents typically contain a single silicon atom bonded to up to four substituent groups, which may be nonreactive, organically reactive, or inorganically reactive. The basic structure of organosilanes is $R_nSi(OR)_{4-n}$, where "R" is an organofunctional group such as an alkyl or aryl group and "OR" is a hydrolysable group such as an alkoxy [6]. The organofunctional part can polymerize with an organic substrate, while the alkoxy groups can react with an inorganic substrate to form covalent bonds between the matrices [7]. Attachment of methoxy, ethoxy, acetoxy, chlorine or nitrogen directly to the silicon atom yields alkoxysilanes (in the case of methoxy and ethoxy), acyloxysilanes, chlorosilanes and silaylamine (silazanes), respectively. These functional groups can undergo rapid hydrolysis in the presence of water, including water-adsorbed moisture, to generate silanol groups (–Si–OH) that can further participate in condensation or surface-binding reactions. For instance, the silanols can react with other silanols to form a very stable siloxane bond (–Si–O–Si–) or with metal hydroxyl groups, e.g., on the surface of mineral fillers, glass or metals to form very stable –Si–O–M bonds [6].

Chemisorption of silanes onto fillers is a two-step process, which starts with the hydrolysis of the silane to produce silanols, followed by a condensation reaction between the resulting silanols and surface hydroxyl groups of the filler. An example is the hydrolysis of trimethoxysilane to form methanol and trisilanol:

$$R - Si(OMe)_3 + 3H_2O \rightarrow R - Si(OH)_3 + 3MeOH \quad (1)$$

The resulting trisilanols undergo condensation reactions with OH groups on the filler surface to form silane–filler covalent bonds:

$$R - Si(OH)_3 + HO - (substrate) \rightarrow R - Si(OH)_2 - O - (substrate) + H_2O \quad (2)$$

The quantity of interactions between silane and the filler is determined by the number of hydroxyl and oxide groups on the surface of the filler in the equilibrium state. These groups play a crucial role in forming hydrogen bonds, electrostatic interactions, or covalent bonding to the filler surface [8]. Hydrolysis and condensation reactions are significantly affected by the pH of the treatment solution. This is because the electrostatic surface potential ($\zeta$-potential) of the filler and the chemical stability of silanol groups depend on the concentration of $H^+$ ions [8,9]. However, the rate-determining step for chemisorption under most conditions is the condensation reaction [8].

Silica is widely used in the rubber industry as a non-carbon black reinforcing filler due to its fine particle size and proven effectiveness in enhancing the mechanical properties of rubber composites, particularly tensile strength, tear resistance, abrasion resistance and hardness [10]. Alumina, on the other hand, is valued for improving the dielectric properties, electrical conductivity [11], and thermal conductivity of rubber composites [12]. In recent years, rubber technologists have shown increasing interest in sourcing silica ($SiO_2$) and alumina ($Al_2O_3$) from natural materials as alternative fillers to lower production costs, improve mechanical properties and address environmental issues related to waste disposal. Coal fly ash (CFA), a low-cost mineral waste by-product of coal combustion, is composed mainly of spherical aluminosilicate glass particles (62%) [13]. These characteristics have attracted growing interest in its use as a filler in rubber composites.

The CFA surface is abundant in hydrophilic –OH groups, and is, therefore, highly polar, making it less compatible with non-polar media. Moreover, the surface –OH groups have a great affinity to form hydrogen bonding with each other, resulting in strong particle-particle agglomeration. This can be prevented by the aid of silane coupling agents, thereby modifying the hydrophilic nature of the CFA surface. Such surface modification not only improves the wettability of CFA in organic media but also improves dispersion in the organic matrix.

Untreated CFA was compared with commercial silica in natural rubber (NR) and styrene–butadiene rubber (SBR) [14]. CFA-filled composites exhibited faster curing and mechanical properties comparable to those of silica-filled systems for up to 30 parts per hundred rubbers (phr), whereas performance declined in both rubber matrices at higher loadings. Enhancement of CFA-NR composites at 30–60 phr through silane treatment of CFA with Si-69 was also reported [10]. In a separate study, up to 40% of carbon black could be replaced with CFA without major losses in tensile strength, elasticity or abrasion resistance, and fractionation was found to be more effective than grinding for improving CFA's reinforcing effect, especially in coarser, highly specific surface area fractions [15]. In our recent study [16], untreated CFA only weakly reinforced cis-1,4-polyisoprene rubber, but CFA surface modification via ammonium sulfate roasting, leaching and silane treatment improved surface area, compatibility, dispersion, and bonding. In addition, in situ silanization outperformed pre-treatment, while blending CFA with carbon black produced synergistic effects, highlighting modified CFA's potential as a sustainable co-filler in rubber composites.

The primary objective of this study was to investigate the effects of solvent system, solution pH, and temperature on the surface functionalization of CFA with (3-aminopropyl) triethoxysilane (APTES) using the One-Factor-at-a-Time (OFAT) method, aiming to improve its interfacial compatibility with polymer matrices. APTES is one of the most widely used aminosilanes due to its high coupling efficiency, low cost, and good solubility in both aqueous and organic solvents [17]. Functionalization occurs through the $–Si(OH)_3$ groups, which bond to inorganic surfaces such as alumina, glass, iron, mica, silica, silica gels, titania, quartz, and zeolites, while the amino group promotes interactions with polymer matrices, thereby enhancing adhesion at the polymer–inorganic interface [18].

## 2. Materials and Methods

### *2.1. Materials*

A commercial ultrafine, air-classified siliceous coal fly ash (CFA) was obtained from Ash Resources (Pty) Ltd., Johannesburg, South Africa. The material had a mean particle size of 3.9–5.0 μm, with 90% of the particles by volume measuring less than 11 μm in diameter. The sample was of the same type as that employed in a previous study [16], thereby ensuring consistency and reproducibility, although it was derived from a different batch.

Acetone ($CH_3COCH_3$; reagent grade, ≥99.5%), ethanol ($CH_3CH_2OH$; reagent grade, ≥99.5%), toluene ($C_6H_5CH_3$; reagent grade, ≥99.5%), sulfuric acid ($H_2SO_4$; reagent grade, 95%–98%), hydrochloric acid (HCl; reagent grade, 37%), and (3-aminopropyl)-triethoxysilane (APTES) were purchased from Sigma-Aldrich (Johannesburg, South Africa). All the chemicals were used as received. Distilled water was used in all experiments.

### *2.2. Silane Coupling of CFA with APTES*

Table 1 summarizes the parameters investigated for the silanization of CFA with APTES using the OFAT method.

**Table 1.** Experimental conditions were studied using the OFAT method.

| Parameter | Variable |
|---|---|
| Solvent (*v*/*v*) | Ethanol/water (80:20), Acetone/water (40:60), Sulphuric acid/water (10:90), Toluene (100:0) |
| Temperature (°C) | 20, 40, 60, 80, 100 |
| pH | 2, 3, 4, 8, 9, 10 |

*Effect of solvent type on silane coupling*. The effect of solvent type on the coupling of silane with CFA was investigated (Table 1). For each experiment, 4 mL of APTES was added to 200 mL of the solvent, and the CFA sample was suspended in the resulting solution. The mixtures were stirred using an overhead stirrer at 1800 rpm while being maintained in a water bath at 80 °C for 5 h. After the reaction, the suspensions were filtered. The residues were washed with 100 mL of the corresponding solvent and subsequently dried in an oven at 80 °C overnight.

*Effect of temperature on silane coupling*. The effect of temperature (20–100 °C) on the coupling of silane with CFA was investigated using a mixture of 200 mL ethanol/water (80:20 *v*/*v*) solution, 4 mL of APTES, and 10.0 g of CFA. At first, the ethanol/water solution was divided equally into two 100 mL portions: 4 mL of APTES was added to one portion, and 10.0 g of CFA to the other. Both beakers were placed in a water bath at the target temperature and stirred at 1800 rpm for 1 h. After this period, the contents of the two beakers were combined, returned to the water bath at the set temperature, and stirred for an additional 5 h. The silanized CFA was then filtered, washed with 100 mL of ethanol/water solution, and dried in an oven at 80 °C overnight.

*Effect of pH on silane coupling*. The effect of pH (2–10) on the silane–CFA coupling reaction was investigated using the procedure described for the temperature experiments. The pH of the two 100 mL portions was adjusted separately to the desired endpoint by dropwise addition of either dilute HCl or APTES. During the course of the reaction, the pH of the suspension was monitored constantly using an Adwa AD1020 multi-parameter pH-ORP-ISE-TEMP bench meter. The reaction was carried out for 5 h, after which the suspension was filtered, washed with 100 mL of ethanol/water solution, and dried in an oven at 80 °C overnight.

### *2.3. Characterization*

*Fourier Transform Infrared Spectroscopy (FTIR).* Infrared spectra were recorded in an evacuated sample compartment on a Bruker Vertex 77v (Bruker, Bremen, Germany), with an attenuated total reflection (ATR) diamond cell. The spectra were measured in the frequency range 4000 $cm^{-1}$ to 400 $cm^{-1}$, and 32 scans of each sample were taken, with a resolution of 2 $cm^{-1}$.

*Scanning Electron Microscopy (SEM).* The morphology of CFA particles was studied on a JEOL JSM-5800LV Scanning Electron Microscope (SEM, JEOL, Tokyo, Japan) operated at 5 kV. CFA particles were mounted on a double-sided tape by dipping carbon stubs into the suspensions. Excess material was removed by gentle blowing with compressed nitrogen. The samples were gold-coated twice using a Sputter-coater (Emitech K550X, Ashford, UK).

*Atomic Force Microscopy (AFM).* AFM imaging was performed using a Bruker Dimension Icon AFM (Bruker, Bremen, Germany). A TESPA-Si doped cantilever tip was employed in tapping mode at a frequency of 0.6 Hz. Samples were prepared by mounting them on a layer of Japan Gold placed on a microscope slide.

## 3. Results and Discussion

### *3.1. Chemical and Mineralogical Compositions of Untreated CFA*

The chemical and mineralogical compositions of various batches of CFA from the same source have been determined by XRF and XRD analyses and were documented in detail in previous studies [13,16]. The sample consisted predominantly of an amorphous aluminosilicate glass phase (62.1 wt.%), with crystalline mullite (31.8 wt.%) and quartz (6.1 wt. %). It was mainly composed of $SiO_2$ (52.6%), $Al_2O_3$ (37.1%), CaO (4.3%), $Fe_2O_3$ (2.9%), MgO (1.4%), and $TiO_2$ (1.6%), while $Cr_2O_3$, CuO, MnO, $Na_2O$, NiO, $V_2O_5$ and $ZrO_2$ were each present at less than 0.1%.

### *3.2. FTIR Investigation of CFA Surface Silanization with APTES*

The FTIR spectrum of untreated CFA (Figure 1) confirmed the presence of both glassy and crystalline phases, evidenced by a broad absorption band between 700 and 1100 $cm^{-1}$. This band was attributed to Si–O–Si and Al–O–Si networks [13,19]. Due to overlapping vibrations of these networks, the individual infrared bands could not be distinctly resolved [20]. The shoulder at 1050 $cm^{-1}$ corresponded to the main –Si–O–M (M = Si or Al) asymmetric stretching band characteristic of untreated CFA [21,22].

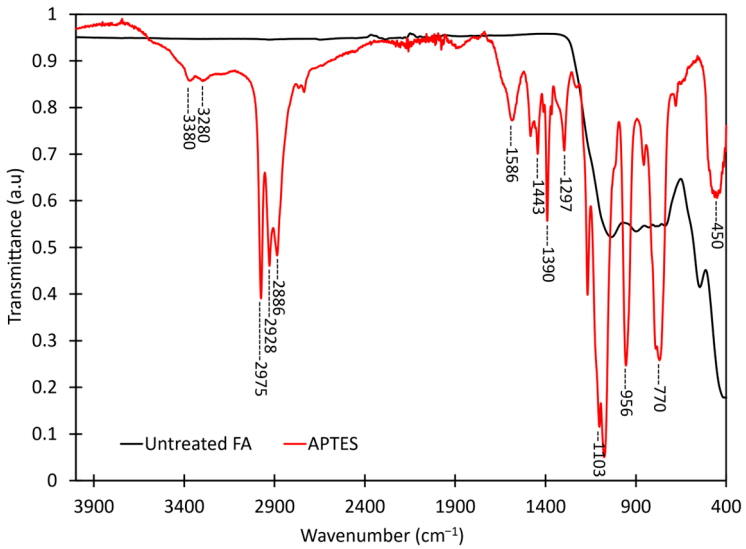


**Figure 1.** FTIR spectra of untreated CFA and pure 3-aminopropyltriethoxysilane (APTES).

APTES is characterized by a bifunctional structure comprising a propyl chain terminated with a primary amine group (–$NH_2$) and a silicon atom linked to three ethoxy groups (–$OCH_2CH_3$) (Figure 2). Its FTIR spectrum is displayed in Figure 1, and the corresponding FTIR band assignments are summarized in Table 2. The spectrum featured intense bands at 770 $cm^{-1}$, 956 $cm^{-1}$, and a doublet at 1076 $cm^{-1}$ and 1103 $cm^{-1}$. These bands corresponded to the stretching and strain modes of ethoxysilane groups (Si–OC, Si–$OCH_2CH_3$) [23,24]. The band at 450 $cm^{-1}$ was attributed to a Si–O rocking band, while the weak band at 1131 $cm^{-1}$ confirmed the presence of the $CH_2$ rocking mode of unreacted ethoxy (Si–$OCH_2CH_3$) groups [25]. The bands at 1297 and 1390 $cm^{-1}$ were assigned to C–H stretching vibrations of $CH_3$ and $CH_2$ groups in the ethoxy functional group [24]. The $NH_2$ scissor vibration appeared at 1586 $cm^{-1}$. $CH_2$ symmetric (at 2886 $cm^{-1}$) and asymmetric (at 2928 $cm^{-1}$) stretching bands reflected the propylamine group of APTES [25,26]. Finally, very weak symmetric and asymmetric NH stretching bands at 3280 and 3380 $cm^{-1}$ arose from the amino groups, which is consistent with their weak dipole moment [25].

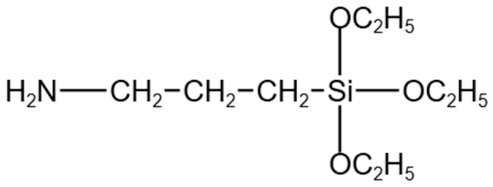


**Figure 2.** The structure of 3-aminopropyltriethoxy silane (APTES).

**Table 2.** FTIR spectral band assignments for APTES.

| Wavenumber ($cm^{-1}$) | Assignment |
|---|---|
| 3380 | symmetric and asymmetric NH stretch |
| 3280 | symmetric and asymmetric NH stretch |
| 2975 | C–H, $SiOCH_2CH_3$ |
| 2928 | C–H, $SiOCH_2CH_3$ |
| 2886 | C–H, $SiOCH_2CH_3$ |
| 1586 | $NH_2$ scissor vibrations, $H_2N$–$CH_2CH_2CH_2$ |
| 1443 | C–H, $CH_2$ |
| 1390 | C–H stretching vibrations in $CH_3$ and $CH_2$ |
| 1297 | C–H stretching vibrations in $CH_3$ and $CH_2$ |
| 1131 | $CH_2$ rocking of unreacted (Si–$OCH_2CH_3$) |
| 1103 | Si–OC, Si–$OCH_2CH_3$ |
| 1076 | Si–OC, Si–$OCH_2CH_3$ |
| 956 | Si–OC, Si–$OCH_2CH_3$ |
| 770 | Si–OC, Si–$OCH_2CH_3$ |
| 450 | Si–O rocking |

Overlap between the FTIR spectra of untreated CFA and APTES was observed in the 400–1300 $cm^{-1}$ region, whereas more pronounced differences appeared in the 1300–4000 $cm^{-1}$ range. This higher wavenumber region was therefore selected to evaluate the extent of silane coupling under different experimental conditions. In particular, the $CH_2$ symmetric and asymmetric stretching bands near 2919 $cm^{-1}$ and 2957 $cm^{-1}$ served as indicators for successful functionalization of FA with APTES. These two band positions for the grafted silane layer exhibited slight shifts relative to those of the pure molecule (2886 and 2928 $cm^{-1}$), which was indicative of modifications in the local chemical environment upon surface grafting. The intensity of these peaks in transmittance mode correlated directly with the concentration of the functional groups, providing confirmation of the coupling process.

*Effect of solvent type on silane coupling*. The choice of solvent in silane coupling with APTES strongly influences the density and conformation of the covalently attached layers [27]. Toluene-based solvents have been used for solution-phase coupling to silica surfaces and have been regarded as performing better than other solvents [28], as their anhydrous, non-aqueous nature prevents premature hydrolysis and uncontrolled polymerization of APTES. In contrast, the presence of water accelerates hydrolysis and self-condensation, reducing the number of APTES molecules available for surface attachment [29]. However, toluene is volatile, flammable, and toxic. To address these issues, alternative solvent systems (acetone/water, ethanol/water, and sulfuric acid/water) have been investigated to reduce toxicity, minimize environmental impact, and potentially enhance APTES coupling efficiency. The FTIR spectra of CFA treated with APTES in various solvent systems are shown in Figure 3a. Silanization was performed in acetone/water (40:60), ethanol/water (80:20), sulfuric acid/water (10:90), and toluene, respectively. Toluene showed the least degree of coupling, probably due to the absence of water that inhibited the hydrolysis of APTES and the subsequent formation of silanol (Si–OH) groups. In contrast,

CFA treated with APTES in aqueous media displayed $CH_2$ symmetric and asymmetric stretching bands at 2919 and 2957 $cm^{-1}$, respectively. These bands, which were absent in the spectra of untreated FA, were attributed to the propylamine chains of APTES, and their presence confirmed the silanization of the CFA surface. The $CH_2$ bands were detected in samples silanized using acetone/water, ethanol/water, and sulfuric acid/water media, but were absent in those treated with toluene. The relative band intensities followed the order: sulfuric acid/water < acetone/water < ethanol/water. Since higher transmittance corresponds to a greater concentration of the associated functional group, these results indicate enhanced APTES adsorption in the ethanol/water solvent system than in the other solvent systems. Accordingly, ethanol/water was selected for all subsequent silane treatments.

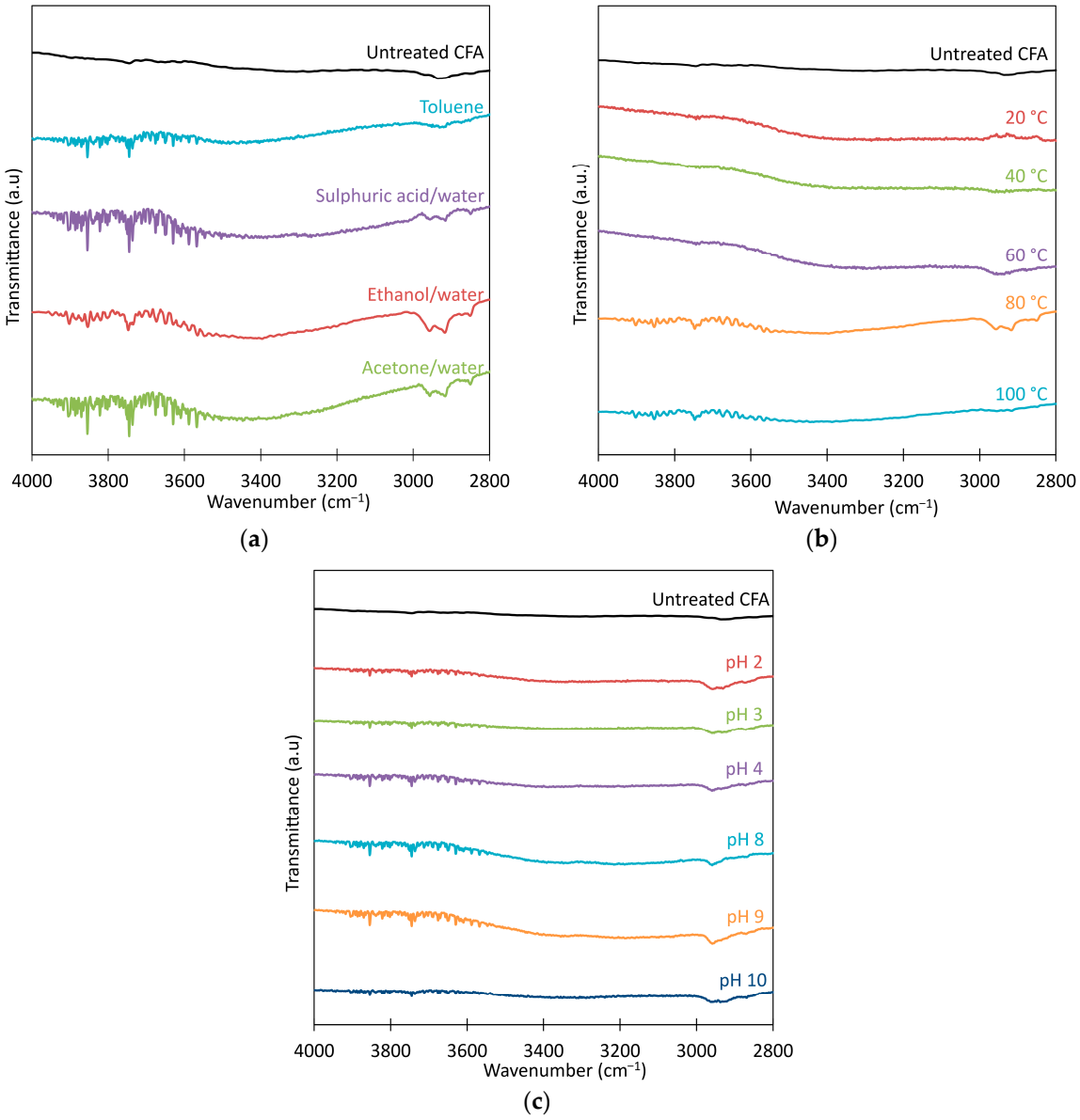


**Figure 3.** FTIR spectra of APTES-treated CFA under different experimental conditions: (**a**) solvent type, (**b**) reaction temperature, and (**c**) pH.

*Effect of temperature on silane coupling*. The effect of temperature on the silanization of CFA with APTES was examined in the ethanol/water solvent system at 20, 40, 60, 80, and 100 °C (Figure 3b). In such solvent systems, increasing temperature generally enhances silane bonding by accelerating the hydrolysis of alkoxyl groups to reactive silanol species

and promoting their subsequent condensation with surface hydroxyl groups, forming strong Si–O–Si covalent bonds [30]. Elevated temperatures also increase molecular motion, thereby increasing the likelihood of collisions between silanol groups and surface hydroxyl sites. This behavior was evident in the present study, with minimal coupling observed at temperatures $\leq$ 60 °C. The maximum degree of coupling occurred at 80 °C, likely due to optimal reaction kinetics, improved solvent interactions and particle dispersion, and efficient removal of by-products such as water and volatiles, resulting in a uniform, defect-free silane layer. At temperatures above 80 °C, competing processes such as premature condensation or thermal degradation of the coupling agent may reduce coupling efficiency [31]. Accordingly, ethanol/water at 80 °C was chosen as the solvent system and temperature condition for the pH-dependent study.

*Effect of pH on silane coupling*. The effect of pH on the silanization of CFA with APTES was examined in the ethanol/water solvent system at 80 °C in the pH values of 2, 3, 4, 8, 9 and 10. The $CH_2$ symmetric and asymmetric stretching peaks reached maximum intensity at pH 9 (Figure 3c). This could be rationalized by considering the amphoteric nature of alumina and silica functional groups on CFA surfaces, whose −OH groups are protonated under acidic conditions and deprotonated under basic conditions [32]. At low pH, extensive protonation generates positively charged surfaces ($-OH_2^+$), whereas at high pH, deprotonation yields negatively charged surfaces ($-O^-$). The point of zero charge (PZC) for alumina occurs near pH 9, which coincides with the natural pH of CFA suspensions [16,33]. At this pH, a significant fraction of surface hydroxyls remains neutral and readily available to react with silanols formed from APTES hydrolysis, minimizing electrostatic repulsion. Hydrolysis and condensation reactions are highly pH-sensitive [34]. Under strongly acidic conditions, hydrolysis is rapid but leads to uncontrolled self-condensation, forming polysiloxanes rather than surface bonds. Under strongly basic conditions, deprotonation reduces surface reactivity and increases electrostatic repulsion. Therefore, pH values around 8–10 offer an optimal balance, with pH 9 providing ideal conditions for silanol reactivity, surface accessibility, and stable APTES grafting [35].

### *3.3. Direct Visualization of CFA Surface Following Silanization with APTES*

The surface of CFA treated with APTES in the ethanol/water solvent system was further characterized through direct visualization using SEM and AFM to support the FTIR findings.

*SEM visualization*. Figure 4a illustrates the characteristic spherical morphology of CFA particles, which exhibited a wide size distribution ranging from sub-micron to >10 μm. Considerable clustering and inter-particle agglomeration were evident. The combination of sphericity and broad particle size distribution is advantageous for filler applications. The low surface-to-volume ratio of spherical particles increases volume loading capacity, reducing shrinkage and lowering material costs due to decreased filler demand. Additionally, small spherical particles can roll over one another, decreasing viscosity and enhancing flow in composites. After APTES treatment (Figure 4b), CFA particles retained their spherical shape and broad size distribution, but particle agglomeration was markedly reduced.

*AFM visualization*. Figure 5 shows the AFM results for representative CFA spheres examined in this study. Figure 5a,b present three-dimensional surface images of untreated and APTES-treated particles, respectively, while Figure 5c,d show the corresponding height profiles. The untreated CFA particle exhibited a largely featureless, smooth surface, whereas the APTES-treated particle displayed a noticeably rough, spiky morphology after silane coupling. These observations provided direct visual evidence of significant surface texture modifications induced by APTES treatment in the ethanol/water solvent system.

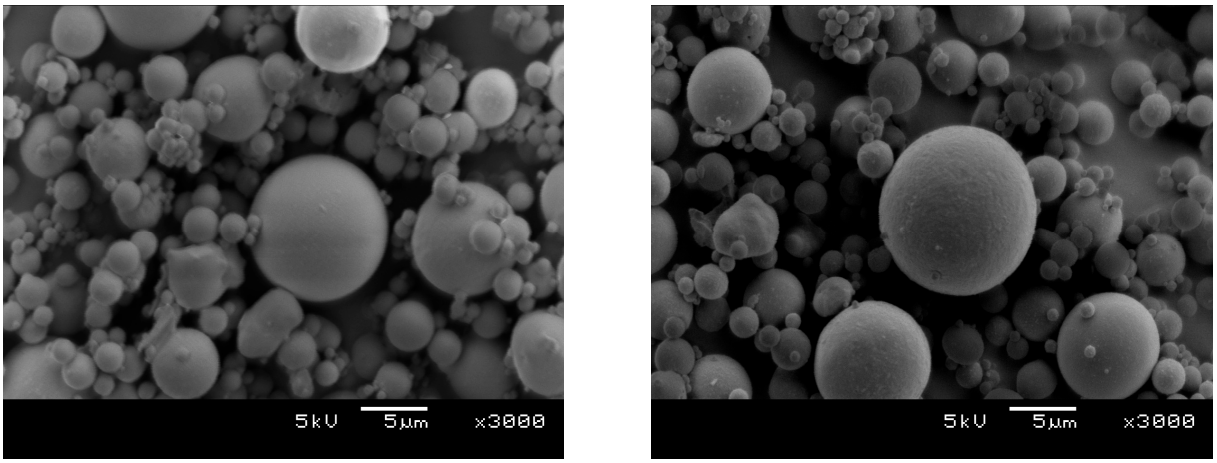


(**a**) (**b**)

**Figure 4.** SEM images of (**a**) untreated CFA and (**b**) APTES-treated CFA.

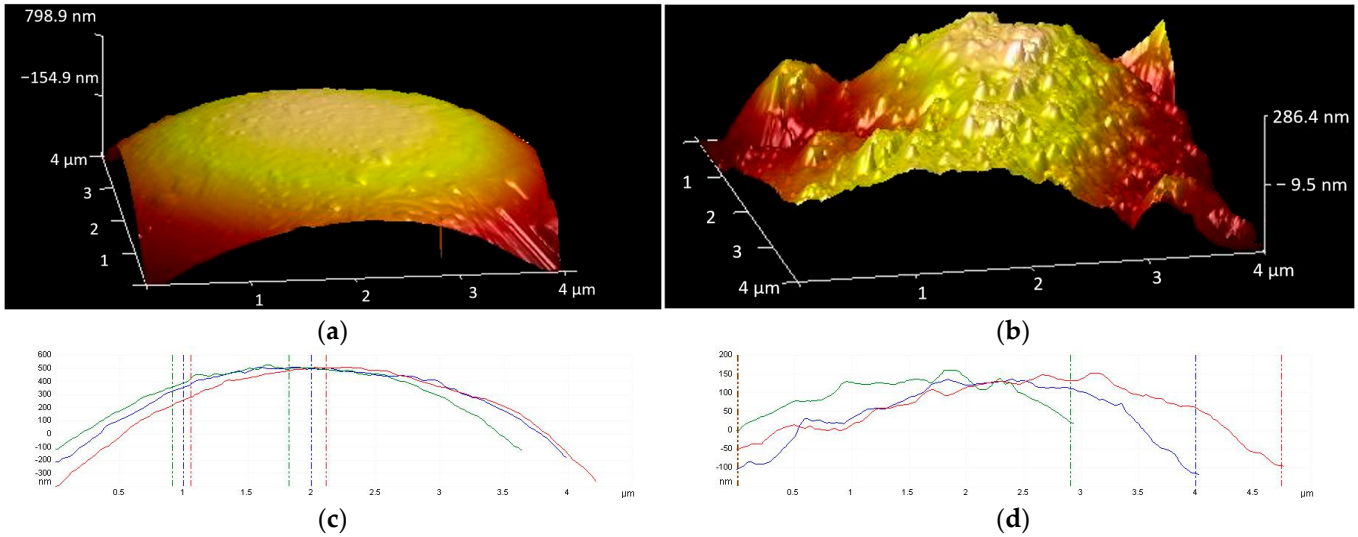


(**a**) (**b**)

(**c**) (**d**)

**Figure 5.** Three-Dimensional AFM topographic images (4 × 4 µm) and height profiles of (**a**,**c**) untreated CFA and (**b**,**d**) APTES-treated CFA.

## 4. Conclusions

This study demonstrated that the surface functionalization of CFA with APTES was strongly influenced by solvent system, reaction temperature, and pH. Solvent mixtures containing water, such as ethanol/water, acetone/water, and sulfuric acid/water, produced better results than toluene because hydrolysis of APTES requires moisture. Ethanol/water mixtures provided the most effective medium for silanization. The coupling efficiency increased with temperature, with maximum functionalization occurring at 80 °C, where favorable kinetics balanced hydrolysis and condensation reactions. The highest degree of grafting was observed at pH 9, corresponding to the point of zero charge of alumina in CFA, which maximized the availability of neutral hydroxyl groups for covalent bonding. FTIR, SEM, and AFM confirmed successful functionalization, reduced agglomeration, and altered surface morphology. These findings highlighted silanized CFA as a promising sustainable filler for rubber composites, with improved dispersion and interfacial compatibility.

**Supplementary Materials:** The following supporting information can be downloaded at: https://www.mdpi.com/article/10.3390/min15111198/s1, Supplementary S1: pH; Supplementary S2: Solvents; Supplementary S3: Temperature; Supplementary S4: Untreated CFA and APTES.

**Author Contributions:** Conceptualization, E.M.v.d.M. and F.J.D.; methodology, D.S.M., E.M.v.d.M. and F.J.D.; validation, D.S.M., E.M.v.d.M. and F.J.D.; formal analysis, D.S.M., G.K., E.M.v.d.M. and F.J.D.; investigation, G.K. and X.W.; resources, E.M.v.d.M.; data curation, E.M.v.d.M.; writing—original draft preparation, D.S.M. and X.W.; writing—review and editing, E.M.v.d.M. and F.J.D.; visualization, D.S.M.; supervision, E.M.v.d.M. and F.J.D.; project administration, E.M.v.d.M.; funding acquisition, E.M.v.d.M. All authors have read and agreed to the published version of the manuscript.

**Funding:** This project was financially supported by the University of Pretoria, the Council for Geoscience, and the National Research Foundation of South Africa (NRF; [93641: 2016; 138020:2022; CPRR240404212107:2025]. Any opinion, finding, conclusion or recommendation expressed in this material is that of the authors and the NRF does not accept any liability in this regard.

**Data Availability Statement:** The raw data supporting the conclusions of this article are provided in the Supplementary Materials.

**Acknowledgments:** The authors thank the University of Pretoria Laboratory for Microscopy and Microanalysis for assistance with SEM and AFM.

**Conflicts of Interest:** The authors declare no conflicts of interest. E.M.v.d.M. received funding from the National Research Foundation of South Africa. The funders had no role in the design of the study; in the collection, analyses, or interpretation of data; in the writing of the manuscript; or in the decision to publish the results.

## Abbreviations

The following abbreviations are used in this manuscript:

| | |
|---|---|
| CFA | coal fly ash |
| APTES | 3-aminopropyltriethoxysilane |
| FTIR | Fourier-transform infrared spectroscopy |
| NR | natural rubber |
| SBR | styrene–butadiene rubber |
| phr | parts per hundred rubber |
| OFAT | one-factor-at-a-Time |
| SEM | scanning electron microscopy |
| AFM | atomic force microscopy |

## References

1. Mancheno-Posso, P.; Dittler, R.F.; Lewis, D.; Juang, P.; Ji, X.; Xu, X.H.; Lynch, D.C. Review of status, trends, and challenges in working with silane and functional silanes. In *Silane: Chemistry, Applications and Performance*; Moriguchi, K., Utagawa, S.S., Eds.; Nova Science Publishers: New York, NY, USA, 2013; pp. 66–87.
2. Indumathy, B.; Sathiyanathan, P.; Prasad, G.; Reza, M.S.; Prabu, A.A.; Kim, H. A comprehensive review on processing, development and applications of organofunctional silanes and silane-based hyperbranched polymers. *Polymers* **2023**, *15*, 2517. [CrossRef] [PubMed]
3. Ahangaran, F.; Navarchian, A.H. Recent advances in chemical surface modification of metal oxide nanoparticles with silane coupling agents: A review. *Adv. Colloid Interface Sci.* **2020**, *286*, 102298. [CrossRef]
4. Xie, Y.; Hill, C.A.; Xiao, Z.; Militz, H.; Mai, C. Silane coupling agents used for natural fiber/polymer composites: A review. *Compos. Part A Appl. Sci. Manuf.* **2010**, *41*, 806–819. [CrossRef]
5. Presto, D.; Meyerhofer, J.; Kippenbrock, G.; Narayanan, S.; Ilavsky, J.; Moctezuma, S.; Sutton, M.; Foster, M.D. Influence of silane coupling agents on filler network structure and stress-induced particle rearrangement in elastomer nanocomposites. *ACS Appl. Mater. Interfaces* **2020**, *12*, 47891–47901. [CrossRef]
6. Goyal, S. Silanes: Chemistry and applications. *J. Indian Prosthodont. Soc.* **2006**, *6*, 14–18. [CrossRef]
7. Matinlinna, J.P.; Lassila, L.V.; Ozcan, M.; Yli-Urpo, A.; Vallittu, P.K. An introduction to silanes and their clinical applications in dentistry. *Int. J. Prosthodont.* **2004**, *17*, 155–164. [PubMed]
8. Naviroj, S.; Culler, S.; Koenig, J.; Ishida, H. Structure and adsorption characteristics of silane coupling agents on silica and E-glass fiber; dependence on pH. *J. Colloid Interface Sci.* **1984**, *97*, 308–317. [CrossRef]

9. Guillet, A. Treatment of fillers with organofunctional silanes, technology and applications. In *Macromolecular Symposia*; Wiley: Hoboken, NJ, USA, 2003; pp. 63–74.
10. Thongsang, S.; Sombatsompop, N. Effect of NaOH and Si69 treatments on the properties of fly ash/natural rubber composites. *Polym. Compos.* **2006**, *27*, 30–40. [CrossRef]
11. Abdelsalam, A.A.; Ward, A.A.; Abdel-Naeem, G.; Mohamed, W.S.; El-Sabbagh, S.H. Effect of alumina modified by silane on the mechanical, swelling and dielectric properties of Al2O3/EPDM/SBR blend composites. *Silicon* **2023**, *15*, 3609–3621. [CrossRef]
12. Yangthong, H.; Nun-Anan, P.; Krainoi, A.; Chaisrikhwun, B.; Karrila, S.; Limhengha, S. Hybrid Alumina–Silica Filler for Thermally Conductive Epoxidized Natural Rubber. *Polymers* **2024**, *16*, 3362. [CrossRef]
13. Van der Merwe, E.M.; Prinsloo, L.C.; Mathebula, C.L.; Swart, H.; Coetsee, E.; Doucet, F. Surface and bulk characterization of an ultrafine South African coal fly ash with reference to polymer applications. *Appl. Surf. Sci.* **2014**, *317*, 73–83. [CrossRef]
14. Sombatsompop, N.; Thongsang, S.; Markpin, T.; Wimolmala, E. Fly ash particles and precipitated silica as fillers in rubbers. I. Untreated fillers in natural rubber and styrene–butadiene rubber compounds. *J. Appl. Polym. Sci.* **2004**, *93*, 2119–2130. [CrossRef]
15. Orczykowski, W.; Bieliński, D.M.; Anyszka, R.; Pędzich, Z. Fly Ash from Lignite Combustion as a Filler for Rubber Mixes. Part I: Physical Valorization of Fly Ash. *Materials* **2022**, *15*, 4869. [CrossRef] [PubMed]
16. Moyo, D.S.; Doucet, F.J.; Hlangothi, S.P.; Woolard, C.D.; Reynolds-Clausen, K.; Kruger, R.A.; van der Merwe, E.M. Physicochemical Surface Modification and Characterisation of Coal Fly Ash for Application in Rubber Composites. *Minerals* **2024**, *14*, 1258. [CrossRef]
17. Branda, F.; Parida, D.; Pauer, R.; Durante, M.; Gaan, S.; Malucelli, G.; Bifulco, A. Effect of the coupling agent (3-aminopropyl) triethoxysilane on the structure and fire behavior of solvent-free one-pot synthesized silica-epoxy nanocomposites. *Polymers* **2022**, *14*, 3853. [CrossRef]
18. Okhrimenko, D.V.; Budi, A.; Ceccato, M.; Cárdenas, M.; Johansson, D.B.; Lybye, D.; Bechgaard, K.; Andersson, M.P.; Stipp, S.L. Hydrolytic stability of 3-aminopropylsilane coupling agent on silica and silicate surfaces at elevated temperatures. *ACS Appl. Mater. Interfaces* **2017**, *9*, 8344–8353. [CrossRef]
19. Caban, R.; Gnatowski, A. Analysis of the Impact of Waste Fly Ash on Changes in the Structure and Thermal Properties of the Produced Recycled Materials Based on Polyethylene. *Materials* **2024**, *17*, 3453. [CrossRef]
20. Nookala, R. Mechanistic Study of Silane Assisted Rubber to Brass Bonding and the Effect of Alkaline Pre Treatment of Aluminum on Silane Performance. Master's Thesis, University of Cincinnati, Cincinnati, OH, USA, 2006.
21. Rees, C.A.; Provis, J.L.; Lukey, G.C.; Van Deventer, J.S. In situ ATR-FTIR study of the early stages of fly ash geopolymer gel formation. *Langmuir* **2007**, *23*, 9076–9082. [CrossRef]
22. Çomo, A.; Ylli, F. FTIR spectroscopic investigation of alkali-activated fly ash: Atest study. *Zast. Mater.* **2018**, *59*, 539–542. [CrossRef]
23. Boerio, F.; Schoenlein, L.; Greivenkamp, J. Adsorption of γ-aminopropyltriethoxysilane onto bulk iron from aqueous solutions. *J. Appl. Polym. Sci.* **1978**, *22*, 203–213. [CrossRef]
24. Pantoja, M.; Martínez, M.; Abenojar, J.; Encinas, N.; Ballesteros, Y. Effect of EtOH/H2O ratio and pH on bis-sulfur silane solutions for electrogalvanized steel joints based on anaerobic adhesives. *J. Adhes.* **2011**, *87*, 688–708. [CrossRef]
25. Aissaoui, N.; Bergaoui, L.; Landoulsi, J.; Lambert, J.-F.; Boujday, S. Silane layers on silicon surfaces: Mechanism of interaction, stability, and influence on protein adsorption. *Langmuir* **2012**, *28*, 656–665. [CrossRef]
26. Boerio, F.; Armogan, L.; Cheng, S. The structure of γ-aminopropyltriethoxysilane films on iron mirrors. *J. Colloid Interface Sci.* **1980**, *73*, 416–424. [CrossRef]
27. Acres, R.G.; Ellis, A.V.; Alvino, J.; Lenahan, C.E.; Khodakov, D.A.; Metha, G.F.; Andersson, G.G. Molecular structure of 3-aminopropyltriethoxysilane layers formed on silanol-terminated silicon surfaces. *J. Phys. Chem. C* **2012**, *116*, 6289–6297. [CrossRef]
28. Miranda, A.; Martínez, L.; De Beule, P.A. Facile synthesis of an aminopropylsilane layer on $Si/SiO_2$ substrates using ethanol as APTES solvent. *MethodsX* **2020**, *7*, 100931. [CrossRef]
29. Munguía-Cortés, L.; Pérez-Hermosillo, I.; Ojeda-López, R.; Esparza-Schulz, J.M.; Felipe-Mendoza, C.; Cervantes-Uribe, A.; Domínguez-Ortiz, A. APTES-functionalization of SBA-15 using ethanol or toluene: Textural characterization and sorption performance of carbon dioxide. *J. Mex. Chem. Soc.* **2017**, *61*, 273–281. [CrossRef]
30. Liu, X.; Zhao, S. Measurement of the condensation temperature of nanosilica powder organically modified by a silane coupling agent and its effect evaluation. *J. Appl. Polym. Sci.* **2008**, *108*, 3038–3045. [CrossRef]
31. Guo, Y.; Wang, Y.-q.; Wang, Z.-m.; Shen, C.-j. Study on the preparation and characterization of high-dispersibility nanosilica. *Sci. Eng. Compos. Mater.* **2016**, *23*, 401–406. [CrossRef]
32. Gunasekara, C.; Law, D.W.; Setunge, S.; Sanjayan, J.G. Zeta potential, gel formation and compressive strength of low calcium fly ash geopolymers. *Constr. Build. Mater.* **2015**, *95*, 592–599. [CrossRef]
33. Veeramasuneni, S.; Yalamanchili, M.; Miller, J. Measurement of interaction forces between silica and α-alumina by atomic force microscopy. *J. Colloid Interface Sci.* **1996**, *184*, 594–600. [CrossRef] [PubMed]

34. Sypabekova, M.; Hagemann, A.; Rho, D.; Kim, S. 3-Aminopropyltriethoxysilane (APTES) deposition methods on oxide surfaces in solution and vapor phases for biosensing applications. *Biosensors* **2022**, *13*, 36. [CrossRef] [PubMed]
35. Suryanarayana, D.; Mittal, K. Effect of pH of silane solution on the adhesion of polyimide to a silica substrate. *J. Appl. Polym. Sci.* **1984**, *29*, 2039–2043. [CrossRef]